

# Right-handed weak currents in neutrinoless $\beta\beta$ decays and ton scale $\beta\beta$ detectors

Hiroyasu Ejiri,<sup>1,\*</sup> Takeshi Fukuyama,<sup>1,†</sup> and Toru Sato<sup>1,‡</sup>

<sup>1</sup>*Research Center for Nuclear Physics, Osaka University, Osaka 567-0047, Japan*

(Dated: January 8, 2025)

Right handed weak currents (RHCs) in the left-right (L-R) symmetric model are examined in neutrinoless double beta decays ( $0\nu$  DBDs) of both  $0^+ \rightarrow 0^+$  and  $0^+ \rightarrow 2^+$  transitions. The structures of the nuclear matrix elements (NMEs) of  $\langle m \rangle$ ,  $\langle \lambda \rangle$  and  $\langle \eta \rangle$ -terms are studied in detail for these two transitions. In case of  $0^+ \rightarrow 0^+$  transition, the enhancement mechanisms of the  $\langle \eta \rangle$  term over the  $\langle \lambda \rangle$  term are shown. The  $\Delta$  isobar contribution to the NME for the transition to the  $2^+$  state is evaluated to be of the order of 10 – 20% of the NME. Measurements of both  $\beta\beta$  and  $\gamma$  rays associated with  $0\nu$  DBDs by means of the ton-scale DBD detectors under construction are used to study the effective RHCs around  $\langle \lambda \rangle \approx 10^{-7}$  and  $\langle \eta \rangle \approx 10^{-10}$ . These values depend on the phase space and the NME with the effective weak coupling of  $g_A^{eff}$ .

## I. INTRODUCTION

Neutrinoless double beta decay ( $0\nu$  DBD) is a realistic probe for studying the neutrino ( $\nu$ ) nature (Majorana or Dirac), the absolute  $\nu$ -mass scale, the right-handed weak current (RHC) and others, which are beyond the standard model (BSM), as discussed in reviews [1–5] and references therein.

In the present work we study the effects of the RHC in the  $0\nu$  DBDs to the ground and excited states, where  $\langle \lambda \rangle$ - and  $\langle \eta \rangle$ -terms in addition to  $\langle m \rangle$ -term appear (Eq. (12)). Based on the neutrino oscillation experiments, the effective Majorana neutrino-mass  $\langle m \rangle$  is around 15–45 meV and 2–5 meV for the inverted mass hierarchy (IH) and the normal mass hierarchy (NH) cases, respectively. Then recent experimental works are concentrated mostly on the light-mass mechanism by measuring the ground-state  $0^+ \rightarrow 0^+$  DBDs [6, 7].

The DBD transition rate depends on the nuclear matrix element (NME). The NME, which reflects the complex nuclear correlations in the DBD nucleus, is crucial to extract the  $\nu$ -mass and the contributions of RHC. The NME, however, depends on the models and the nuclear parameters used there [8–12]. One critical parameter is the effective axial-vector weak coupling  $g_A^{eff}$ , which is much quenched in a nucleus due to the various kinds of the nucleonic and non-nucleonic correlations [13–15].

Recent high-sensitivity experiments have excluded the larger  $\nu$ -mass region of  $\langle m \rangle \geq 100$ –200 meV if the NME is around  $M_m \approx 2$ –3. Then they are going to build higher-sensitivity and larger-scale DBD detectors to search for the neutrino mass in the IH neutrino-mass region around  $\langle m \rangle \approx 30$  meV. Since the minimum neutrino-mass to be measured is proportional to  $(B/N)^{1/4}$  with  $N$  being the total amounts of the DBD isotopes used in the detector and  $B$  being the backgrounds, one needs ton-scale ( $N \approx$  tons) detectors to measure the IH neutrino-mass and even multi-10 ton scale DBD detectors for the NH neutrino mass. Accordingly, one might anticipate that the ton-scale DBD detectors under construction may not be quite effective if the neutrino mass spectrum is of NH without RHC.

From the theoretical view point of grand unified theories, our results prefer the NH to the IH: that is, inputting the observed lepton masses and the PMNS angles into the model, we compare the outputs of quark masses and CKM matrices in the model with the observed data, and obtained  $\chi^2 \leq 1$  for the NH case and  $\chi^2 > 200$  for the IH case [16]. On the other hand, recent measurements of baryonic acoustic oscillations of cosmic microwave background constrain [17–19]  $\sum_i m_{\nu i} < 0.072$  eV at 95% C.L. This bound disfavors IH at  $3\sigma$  [20]. If this is the case, the future ton-scale DBD detectors may find no signal without RHC. The present paper aims to report for the first time how the ton-scale DBD detectors are used to study the RHC of the current interest by measuring both  $0\nu$  DBDs to the  $0^+$  ground and  $2^+$  excited states. The RHCs to be studied are the  $\langle \lambda \rangle$  and  $\langle \eta \rangle$  in the region of  $10^{-(6-7)}$  and  $10^{-(9-10)}$  regions, respectively. Then the DBD signal in the  $0^+$  ground state is due to either  $\langle \lambda \rangle$  or  $\langle \eta \rangle$ , or both of them, while that in the  $2^+$  one is exclusively due to  $\langle \lambda \rangle$ , as will be discussed in Sec. 3 and Sec. 4. From these experiments we obtain the values on the parameters included in  $\langle m \rangle$ ,  $\langle \lambda \rangle$  and  $\langle \eta \rangle$  mechanisms in BSM physics.

DBD detectors to be discussed in the present work are  $\beta - \gamma$  detectors to make it possible to separate the excited-state decay from the ground state decay and to reduce considerably back-ground contributions to both the ground and excited state DBD studies, as shown in early works with ELEGANT experiments [21, 22].

\* ejiri@rcnp.osaka-u.ac.jp

† fukuyama@rcnp.osaka-u.ac.jp

‡ tsato@rcnp.osaka-u.ac.jp

Actually, recent  $\nu$ -mass DBD experiments have been made mostly on DBDs to the  $0^+$  ground state in medium heavy nuclei with the large  $Q$ -value around 2-3 MeV since the  $\nu$ -mass DBD is exclusively due to the  $0^+$  ground state. Detectors used are mostly calorimetric detectors to measure the total DBD energy, but do not measure individual  $2^-$   $\beta$ -ray tracks to identify the DBD processes, the mass, the RHC  $\lambda$ , and  $\eta$  ones.

This paper is organized as follows. The theoretical aspects of the RHC DBD are discussed briefly in section 2. The RHC NMEs for the  $0^+$  ground and  $2^+$  excited state transitions are discussed in section 3. Here we include brief discussions on the possible contribution of the  $\Delta$  isobar to the RHC NMEs to the  $2^+$  excited state. Experimental sensitivities for measuring the  $\lambda$  and  $\eta$  RHCs and experimental merits of measuring both  $\beta\beta$  and  $\gamma$  rays are explained in section 4. Finally remarks on the future RHC DBD works are briefly given in section 5.

## II. THEORETICAL ASPECTS OF RHC DBDS

We use the notations of [23] for the detailed applications of Left-Right (L-R) symmetric model. The weak Hamiltonian is given by

$$H_W = \frac{G_F \cos \theta_c}{\sqrt{2}} \left[ j_L^\mu \tilde{J}_{L\mu}^\dagger + j_R^\mu \tilde{J}_{R\mu}^\dagger \right] + H.c. \quad (1)$$

Here  $j_\mu$  ( $J_\mu$ ) indicates the leptonic (hadronic) current, and the L- and R-handed leptonic currents,  $j_{L\mu}$  and  $j_{R\mu}$ , are given by

$$\begin{aligned} j_{L\alpha} &= \sum_{l=e,\mu,\tau} \bar{l}(x) \gamma_\alpha (1 - \gamma_5) \nu_{lL}(x) \\ &\equiv \sum \bar{l}(x) \gamma_\alpha 2P_L \nu_{lL}(x), \end{aligned} \quad (2)$$

$$\begin{aligned} j_{R\alpha} &= \sum_{l=e,\mu,\tau} \bar{l}(x) \gamma_\alpha (1 + \gamma_5) N_{lR}(x) \\ &\equiv \sum \bar{l}(x) \gamma_\alpha 2P_R N_{lR}(x), \end{aligned} \quad (3)$$

where  $\nu_{lL}$  ( $N_{lR}$ ) are L-handed (R-handed) weak eigenstates of the neutrinos, and

$$\tilde{J}_L^\mu(\mathbf{x}) = J_L^\mu(\mathbf{x}) + \kappa J_R^\mu(\mathbf{x}), \quad (4)$$

$$\tilde{J}_R^\mu(\mathbf{x}) = \eta J_L^\mu(\mathbf{x}) + \lambda J_R^\mu(\mathbf{x}). \quad (5)$$

The neutrino mass matrix is [24–27]

$$M_\nu = \begin{pmatrix} M_L & M_D^T \\ M_D & M_R \end{pmatrix} \approx \begin{pmatrix} 0 & M_D^T \\ M_D & M_R \end{pmatrix}. \quad (6)$$

Thus we have the extended Fermi couplings (1). In (2) and (3),  $\nu_{lL}$  ( $N_{lR}$ ) are L-handed (R-handed) weak eigenstates of the neutrinos. Using  $3 \times 3$  blocks  $U, V, X, Y$ , the mass eigenstates  $\nu'$ ,  $N'$  are given as

$$\begin{pmatrix} \nu \\ (N_R)^c \end{pmatrix}_L = \begin{pmatrix} U & X \\ V^* & Y \end{pmatrix} \begin{pmatrix} \nu' \\ N' \end{pmatrix}_L \equiv \mathcal{U} \begin{pmatrix} \nu' \\ N' \end{pmatrix}_L. \quad (7)$$

That is,

$$(\nu_L)_\alpha = U_{\alpha i} \nu'_i + X_{\alpha I} N'_I, \quad (N_R)_\alpha^c = V_{\alpha i}^* \nu'_i + Y_{\alpha I} N'_I, \quad (8)$$

where  $\alpha$  ( $i$ ) are the flavour (mass) eigenstates.

$$\mathcal{U}^T M_\nu \mathcal{U} = \begin{pmatrix} m_{light} & 0_{3 \times 3} \\ 0_{3 \times 3} & M_{heavy} \end{pmatrix}. \quad (9)$$

$$m_{light} = -M_D^T M_R^{-1} M_D \quad (10)$$

From GUT, if we adopted very naive order estimation neglecting flavour indices,  $M_D$  is of order of the top quark mass, and  $M_R$  is of order of  $10^{14}$  GeV and the effect of RHC is not observable. However, we can realize the TeV

scale seesaw [28] in the  $SU(2)_L \times SU(2)_R \times U(1)_{B-L}$  model [29]. The transition rate (inverse of the half-life  $T_{1/2}^J$ ) for  $0^+ \rightarrow J^+$  ( $J = 0, 2$ ) is given as [1, 30–34]

$$\begin{aligned} \Gamma^{(J)} &\equiv \frac{1}{T_{1/2}^J} = C_{mm}^{(J)} \left( \frac{\langle m \rangle}{m_e} \right)^2 + C_{m\lambda}^{(J)} \frac{\langle m \rangle}{m_e} \langle \lambda \rangle \\ &+ C_{m\eta}^{(J)} \frac{\langle m \rangle}{m_e} \langle \eta \rangle + C_{\lambda\lambda}^{(J)} \langle \lambda \rangle^2 \\ &+ C_{\eta\eta}^{(J)} \langle \eta \rangle^2 + C_{\lambda\eta}^{(J)} \langle \lambda \rangle \langle \eta \rangle. \end{aligned} \quad (11)$$

Here  $C_{ab}^{(0)}$  includes the NME and the phase space integral. The other parts include the  $\nu$ -mass and the BSM physics. The effective couplings  $\langle \eta \rangle$  and  $\langle \lambda \rangle$  are given as

$$\langle m \rangle = \left| \sum_i U_{ei}^2 m_i \right|, \quad \langle \lambda \rangle = \lambda \left| \sum_j U_{ej} V_{ej} \right|, \quad \langle \eta \rangle = \eta \left| \sum_j U_{ej} V_{ej} \right|. \quad (12)$$

The constants  $\lambda$  and  $\eta$  in (1) are related to the mass eigenvalues of the weak bosons in the L and R-handed gauge sectors ( $W_L, W_R$ ) as follows [35]

$$W_L^+ = W_1^+ \cos \zeta - W_2 \sin \zeta e^{-i\alpha}, \quad (13)$$

$$W_R = W_1^+ \sin \zeta e^{i\alpha} + W_2^+ \cos \zeta, \quad (14)$$

$$\frac{G_F}{\sqrt{2}} = \frac{g^2}{8} \cos^2 \zeta \frac{M_{W_1}^2 \tan^2 \zeta + M_{W_2}^2}{M_{W_1}^2 M_{W_2}^2}, \quad (15)$$

$$\lambda = \frac{M_{W_1}^2 + M_{W_2}^2 \tan^2 \zeta}{M_{W_1}^2 \tan^2 \zeta + M_{W_2}^2}, \quad (16)$$

$$\eta = -\frac{(M_{W_2}^2 - M_{W_1}^2) \tan \zeta}{M_{W_1}^2 \tan^2 \zeta + M_{W_2}^2}. \quad (17)$$

Here  $M_{W_1}$  and  $M_{W_2}$  are the masses of the mass eigenstates  $W_1$  and  $W_2$ , respectively, and  $\zeta$  is the mixing angle which relates the mass eigenstates and the gauge eigenstates. We are considering L-R symmetric model. The gauge boson masses are [35]

$$M_W^2 = \begin{pmatrix} \frac{1}{2} g^2 (\kappa^2 + \kappa'^2 + 2v_L^2) & -g^2 \kappa \kappa' e^{-i\alpha} \\ -g^2 \kappa \kappa' e^{i\alpha} & g^2 v_R^2 \end{pmatrix}. \quad (18)$$

Here the the Yukawa coupling between quark doublets (and lepton doublets) and bi-doublet Higgs is given by

$$\mathcal{L}_Y = \bar{Q}_{Li} (Y_{ij} \Phi + Y'_{ij} \tilde{\Phi}) Q_{Rj} + H.c. \quad (19)$$

with

$$\langle \Phi \rangle = \begin{pmatrix} \kappa & 0 \\ 0 & \kappa' e^{i\alpha} \end{pmatrix}, \quad \text{and} \quad \tilde{\Phi} = \tau_2 \Phi^* \tau_2. \quad (20)$$

Thus this model is the "minimal" L-R symmetric model. We consider this model to clarify the essence of L-R symmetric model in DBD. However, the quark mixing angle is almost diagonal and if we assume

$$\kappa \gg \kappa', \quad \text{and} \quad Y_{ij} \gg Y'_{ij}, \quad (21)$$

then they are related with more familiar quantities,

$$\kappa \approx v_u, \quad \kappa' \approx v_d, \quad \frac{1}{\sqrt{2}} (\kappa^2 + \kappa'^2) = v_{ew}^2 \quad (22)$$

and the L-R weak boson mixing angle becomes

$$\tan 2\zeta = -\frac{2\kappa\kappa'}{v_R^2} \approx \frac{2v_u v_d}{v_R^2} = -4\xi \left( \frac{M_{WL}}{M_{WR}} \right)^2 \quad (23)$$

with

$$\xi \equiv \kappa'/\kappa \approx v_d/v_u \equiv 1/\tan\beta \quad (24)$$

[36] and

$$M_{W2} = g_R v_R \geq 3.7 \text{ TeV} \quad (25)$$

[37], where the symbol  $\approx$  implies to adopt the assumption of (21). In the L-R symmetric model, we set  $g_L = g_R$ , which indicates further unification of at least rank five GUT, including SU(3) color.  $\tan\beta$  is constrained from the fact that the Yukawa coupling is renormalizable up to the GUT scale,

$$0.5 \leq \tan\beta \leq 60. \quad (26)$$

That is, the upper limit (lower limit) appears from the renormalizability of bottom (top) Yukawa coupling in GUT. As will be shown in Sec. 4, we note that the RHC regions to be studied are  $\langle \lambda \rangle \approx 10^{-7}$  and  $\langle \eta \rangle \approx 10^{-10}$ . If we adopt the approximation (22), one may get

$$\lambda \approx \left(\frac{M_1}{M_2}\right)^2 \text{ and } \eta \approx -\tan\zeta \approx \left(\frac{M_L^2}{M_R^2}\right) \frac{1}{\tan\beta} \approx \frac{\lambda}{\tan\beta}. \quad (27)$$

### III. RHC DBD NMES FOR THE GROUND $0^+$ AND EXCITED $2^+$ STATES

#### A. Transition amplitude of $0\nu$ DBD

The transition amplitude  $I \rightarrow F + e_{p_1, s_1} + e_{p_2, s_2}$  is given by the second order perturbation of  $H_W$  following Ref. [38] as,

$$\begin{aligned} R_{0\nu} = & \frac{4}{\sqrt{2}} \left(\frac{G \cos\theta_c}{\sqrt{2}}\right)^2 \sum_{\alpha, \beta, i} \int d\mathbf{x} d\mathbf{y} \int \frac{d\mathbf{k}}{(2\pi)^3} e^{-i\mathbf{k}\cdot\mathbf{r}} \frac{-1}{2\omega} \\ & \times [(\bar{e}_{\mathbf{p}_2, s_2}(\mathbf{y}) \gamma^\mu P_\beta (\gamma_0 \omega - \boldsymbol{\gamma} \cdot \mathbf{k} + m_i) P_\alpha \gamma^\nu e_{\mathbf{p}_1, s_1}^c(\mathbf{x})) \langle F | \tilde{J}_\beta^{\nu\dagger}(\mathbf{y}) \frac{1}{E_I - (H_{st} + \omega + e_1)} \tilde{J}_\beta^{\mu\dagger}(\mathbf{x}) | I \rangle \\ & - (\bar{e}_{\mathbf{p}_2, s_2}(\mathbf{y}) \gamma^\mu P_\beta (\gamma_0 \omega + \boldsymbol{\gamma} \cdot \mathbf{k} - m_i) P_\alpha \gamma^\nu e_{\mathbf{p}_1, s_1}^c(\mathbf{x})) \langle F | \tilde{J}_\beta^{\nu\dagger}(\mathbf{y}) \frac{1}{E_I - (H_{st} + \omega + e_2)} \tilde{J}_\beta^{\mu\dagger}(\mathbf{x}) | I \rangle]. \quad (28) \end{aligned}$$

Here the four momentum of the exchanged neutrino is  $k^\mu = (\omega, \mathbf{k})$ ,  $\mathbf{r} = \mathbf{x} - \mathbf{y}$  and  $e_i$  is energy of electron,  $\omega = \sqrt{\mathbf{k}^2 + m_\nu^2}$ .  $|I\rangle, |F\rangle$  are state vector of the initial and the final hadron states and  $H_{st}$  is Hamiltonian of strong interaction. It is noticed that at this stage hadron current  $\tilde{J}_\alpha^\mu$  is given in terms of current quark and initial and final state vector can be nuclear states or any hadronic states.

To simplify the derivation, we assume that the neutrino energy  $\omega$  dominates the energy denominator  $E_I - (H_{st} + \omega + e_i)$ .  $R_{0\nu}$  is then expressed as

$$R_{0\nu} = \frac{i}{4\pi} \frac{4}{\sqrt{2}} \left(\frac{G \cos\theta_c}{\sqrt{2}}\right)^2 \langle F | \mathcal{M} | I \rangle \quad (29)$$

with

$$\mathcal{M} = \sum_{\alpha, \beta, i} \int d\mathbf{x} d\mathbf{y} \frac{h(r)}{r^2} \bar{e}_{\mathbf{p}_2, s_2}(\mathbf{y}) \tilde{J}_\beta^\dagger(\mathbf{y}) P_\beta(\mathbf{r} \cdot \boldsymbol{\gamma}) P_\alpha \tilde{J}_\alpha^\dagger(\mathbf{x}) e_{\mathbf{p}_1, s_1}^c(\mathbf{x}). \quad (30)$$

Here  $h(r)$  is given as

$$h(r) = -\frac{4\pi}{(2\pi)^3} r \frac{d}{dr} \int d\mathbf{k} \frac{e^{-i\mathbf{k}\cdot\mathbf{r}}}{\omega^2} \sim \frac{1}{r}. \quad (31)$$

Now, the  $\eta$  and  $\lambda$  dependence of  $\mathcal{M}$  are clearly given as

$$\mathcal{M} = \int d\mathbf{x} d\mathbf{y} \frac{h(r)}{r^2} \bar{e}_{\mathbf{p}_2, s_2}(\mathbf{y}) \mathcal{O} e_{\mathbf{p}_1, s_1}^c(\mathbf{x}), \quad (32)$$

with

$$\begin{aligned} \mathcal{O} = & \langle \eta \rangle [(\dot{V}(\mathbf{y})(\mathbf{r} \cdot \boldsymbol{\gamma})\dot{V}(\mathbf{x}) + \dot{A}(\mathbf{y})(\mathbf{r} \cdot \boldsymbol{\gamma})\dot{A}(\mathbf{x})) - (\dot{V}(\mathbf{y})(\mathbf{r} \cdot \boldsymbol{\gamma})\dot{A}(\mathbf{x}) + \dot{A}(\mathbf{y})(\mathbf{r} \cdot \boldsymbol{\gamma})\dot{V}(\mathbf{x}))] \\ & + \langle \lambda \rangle [(\dot{V}(\mathbf{y})(\mathbf{r} \cdot \boldsymbol{\gamma})\dot{V}(\mathbf{x}) - \dot{A}(\mathbf{y})(\mathbf{r} \cdot \boldsymbol{\gamma})\dot{A}(\mathbf{x})) - (\dot{V}(\mathbf{y})(\mathbf{r} \cdot \boldsymbol{\gamma})\dot{A}(\mathbf{x}) - \dot{A}(\mathbf{y})(\mathbf{r} \cdot \boldsymbol{\gamma})\dot{V}(\mathbf{x}))\gamma_5]. \end{aligned} \quad (33)$$

The difference between the  $\langle \eta \rangle$ - and  $\langle \lambda \rangle$ -terms is transparent that relative sign between vector current  $V - V$  and axial vector current  $A - A$  and interference term of vector and axial vector term  $V - A$  and  $A - V$ . Furthermore,  $\gamma_5$  of  $\langle \lambda \rangle$ -term modifies even-odd structure of lepton Dirac matrix. The formula can be used both for  $0^+ \rightarrow 0^+$  and  $0^+ \rightarrow 2^+$  nuclear DBD. Since the angular momentum  $L = 1$  and parity  $-1$  are carried by neutrino,  $s_{1/2}$  and  $p_{1/2}$  partial waves of the electron contributes to the  $0^+ \rightarrow 0^+$  transition. However, as first noticed in Ref. [39] and discussed in Ref. [23], magnetization current  $\nabla \times \boldsymbol{\mu}$  with the  $(s_{1/2})^2$  electrons enhances the sensitivity of  $\eta$  term through the  $V - A$  interference term.

The enhancement mechanism of the  $\langle \eta \rangle$ -term for  $0^+ \rightarrow 0^+$  DBD does not work for  $0^+ \rightarrow 2^+$ . In order to carry  $J = 2$ , electrons have to be at least  $s_{1/2}$  and  $p_{3/2}$  orbits. Sensitivity of the  $\langle \eta \rangle$ -term is similar to that of  $\langle \lambda \rangle$ -term for  $0^+ \rightarrow 2^+$  DBD, while  $0^+ \rightarrow 0^+$  DBD is particularly sensitive to the  $\langle \eta \rangle$ -term.

### B. Effective operator for $0^+ \rightarrow 2^+$ transition

The outline of the derivation of the transition amplitude of angular momentum  $J = 2$  of RHC DBD is briefly described. Using standard partial wave expansion of the scattering wave functions of electron [40], leading order contribution of  $s_{1/2}$  and  $p_{3/2}$  states are taken as follows,

$$\bar{e}_{p_2, s_2}(\mathbf{y}) = \chi_{s_2}^\dagger(g_{-1}^*(p_2, y), -f_1^*(p_2, y)(\hat{p}_2 \cdot \boldsymbol{\sigma})), \quad (34)$$

$$e_{p_1, s_1}^c(\mathbf{x}) = \begin{pmatrix} -if_2^*(p_1, x)[3(\hat{x} \cdot \hat{p}_1)(\hat{p}_1 \cdot \boldsymbol{\sigma}) - (\hat{x} \cdot \boldsymbol{\sigma})] \\ ig_{-2}^*(p_1, x)[3(\hat{x} \cdot \hat{p}_1) - (\hat{x} \cdot \boldsymbol{\sigma})(\hat{p}_1 \cdot \boldsymbol{\sigma})] \end{pmatrix} \chi_{s_1}^c, \quad (35)$$

with  $\chi_s^c = i\sigma_2\chi_s$ .  $\hat{x}$  is a unit vector  $\mathbf{x}/|\mathbf{x}|$ . Matrix element  $\mathcal{M}$  is given by the sum of the each electron wave functions as

$$\mathcal{M} = \mathcal{M}^{-2-1} + \mathcal{M}_{21} + \mathcal{M}_2^{-1} + \mathcal{M}_1^{-2}. \quad (36)$$

Here  $\mathcal{M}^{ij}$  includes electron wave function  $f_j^i$  defined in Ref. [38] where a superscript  $i$  (a subscript  $j$ ) etc. indicate that  $g_i^{(-)}$  ( $f_j^{(-)}$ ) should be taken. For example  $f^{-2-1} = g_{-2}(p_1, R)g_{-1}(p_2, R)$ , where  $R$  is nuclear radius.  $f^{-2-1}$  and  $f_{21}$  contribute to the phase space factor  $G_1$ , while  $f_2^{-1}$  and  $f_1^{-2}$  contribute to  $G_2$ .  $G_1$  and  $G_2$  are defined in Refs. [41, 43].  $\mathcal{M}^{-2-1}$  and  $\mathcal{M}_{21}$ , which are the odd element of Dirac matrix  $\mathcal{O}$ , give effective rank 2 operators of  $\langle \lambda \rangle M_\lambda - \langle \eta \rangle M_\eta$ .  $\mathcal{M}_2^{-1}$  and  $\mathcal{M}_1^{-2}$  from the even element of  $\mathcal{O}$  give  $\langle \eta \rangle M'_\eta$ .

Matrix element  $\mathcal{M}^{-2-1}$  and  $\mathcal{M}_2^{-1}$  are given as

$$\begin{aligned} \mathcal{M}^{-2-1} = & -i \frac{f^{-2-1*}}{R} \int d\mathbf{x} d\mathbf{y} \frac{h(r)}{r^2} \chi_{s_2}^\dagger [\langle \eta \rangle (M_{VV} + M_{AA}) + \langle \lambda \rangle (M_{VV} - M_{AA} + M_{VA-})] \\ & \times (3(\mathbf{x} \cdot \hat{p}_1) - (\mathbf{x} \cdot \boldsymbol{\sigma})(\hat{p}_1 \cdot \boldsymbol{\sigma})) \chi_{s_1}^c, \end{aligned} \quad (37)$$

$$\mathcal{M}_2^{-1} = i \frac{f_2^{-1*}}{R} \int d\mathbf{x} d\mathbf{y} \frac{h(r)}{r^2} \chi_{s_2}^\dagger \langle \eta \rangle M_{VA+} (3(\mathbf{x} \cdot \hat{p}_1)(\hat{p}_1 \cdot \boldsymbol{\sigma}) - (\mathbf{x} \cdot \boldsymbol{\sigma})) \chi_{s_1}^c, \quad (38)$$

where  $M_{VV}, M_{AA}, M_{VA\pm}$  are

$$M_{VV} = V_0(\mathbf{y})\mathbf{r} \cdot \boldsymbol{\sigma} V_0(\mathbf{x}), \quad (39)$$

$$M_{AA} = (\mathbf{A}(\mathbf{y}) \cdot \boldsymbol{\sigma})(\mathbf{r} \cdot \boldsymbol{\sigma})(\mathbf{A}(\mathbf{x}) \cdot \boldsymbol{\sigma}), \quad (40)$$

$$M_{VA\pm} = V_0(\mathbf{y})(\mathbf{r} \cdot \boldsymbol{\sigma})(\mathbf{A}(\mathbf{x}) \cdot \boldsymbol{\sigma}) \pm (\mathbf{A}(\mathbf{y}) \cdot \boldsymbol{\sigma})(\mathbf{r} \cdot \boldsymbol{\sigma})V_0(\mathbf{x}). \quad (41)$$

Rewriting  $\mathcal{M}$ , the multipole operator for hadron is written by the product of hadron and lepton irreducible tensors of rank 2. Here we show  $\mathcal{M}^{-2-1}$ , which include necessary operator for DBD of  $\Delta_{1232}$ . The matrix element is rewritten in terms of hadron tensor  $\mathcal{H}$  and lepton tensor  $\mathcal{L}$  of rank  $J = 2$  as

$$\mathcal{M}^{-2-1} = -i \frac{f^{-2-1*}}{R} \frac{3\sqrt{5}}{2} [\mathcal{H} \otimes \mathcal{L}]^{(0)}, \quad \mathcal{M}_2^{-1} = i \frac{f_2^{-1*}}{R} \frac{3\sqrt{5}}{2} [\mathcal{H}' \otimes \mathcal{L}']^{(0)}. \quad (42)$$

The lepton tensor, which is independent of nuclear coordinate is

$$\mathcal{L} = \chi_{s_2}^\dagger [\hat{p}_1 \otimes \boldsymbol{\sigma}]^{(2)} \chi_{s_1}^c, \quad \mathcal{L}' = \chi_{s_2}^\dagger ([\hat{p}_1 \otimes \hat{p}_1]^{(2)} + \sqrt{\frac{3}{2}} [[\hat{p}_1 \otimes \hat{p}_1]^{(2)} \otimes \boldsymbol{\sigma}]^{(2)}) \chi_{s_1}^c \quad (43)$$

and the hadron tensor is

$$\mathcal{H} = \langle \eta \rangle [h_{VV} + h_{AA}] - \langle \lambda \rangle [-h_{VV} + h_{AA} - h_{VA-}], \quad \mathcal{H}' = \langle \eta \rangle h_{VA+}. \quad (44)$$

Here

$$h_{VV} = \int d\mathbf{x} d\mathbf{y} h(r) V_0(\mathbf{y}) V_0(\mathbf{x}) [\hat{r} \otimes \hat{r}]^{(2)}, \quad (45)$$

$$h_{AA} = \int d\mathbf{x} d\mathbf{y} h(r) \left( \frac{2}{3} [\mathbf{A}(\mathbf{y}) \otimes \mathbf{A}(\mathbf{x})]^{(2)} - \frac{1}{3} \mathbf{A}(\mathbf{y}) \cdot \mathbf{A}(\mathbf{x}) [\hat{r} \otimes \hat{r}]^{(2)} - \sqrt{\frac{7}{3}} [[\mathbf{A}(\mathbf{y}) \otimes \mathbf{A}(\mathbf{x})]^{(2)} \otimes [\hat{r} \otimes \hat{r}]^{(2)}]^{(2)} \right), \quad (46)$$

$$h_{VA-} = -\sqrt{\frac{3}{2}} \int d\mathbf{x} d\mathbf{y} h(r) [(V_0(\mathbf{y}) \mathbf{A}(\mathbf{x}) + \mathbf{A}(\mathbf{y}) V_0(\mathbf{x})) \otimes [\hat{r} \otimes \hat{r}]^{(2)}]^{(2)}, \quad (47)$$

$$h_{VA+} = \int d\mathbf{x} d\mathbf{y} h(r) \frac{r_+}{r} [(V_0(\mathbf{y}) \mathbf{A}(\mathbf{x}) - \mathbf{A}(\mathbf{y}) V_0(\mathbf{x})) \otimes \left( \frac{1}{\sqrt{2}} [\hat{r} \otimes \hat{r}_+]^{(1)} - \sqrt{\frac{3}{2}} [\hat{r} \otimes \hat{r}_+]^{(2)} \right)]^{(2)} \quad (48)$$

with  $\mathbf{r}_+ = \mathbf{x} + \mathbf{y}$ .

Taking the impulse approximation of the nuclear current  $V_0(\mathbf{x}) = \sum_i \tau_i^+ \delta(\mathbf{r}_i - \mathbf{x})$  and  $\mathbf{A}(\mathbf{x}) = \sum_i g_A \tau_i^+ \boldsymbol{\sigma}_i \delta(\mathbf{r}_i - \mathbf{x})$ , the half-life [43] derived at first in Ref. [41] is given as,

$$(T_{1/2})^{-1} = G_1 | \langle \lambda \rangle M'_\lambda - \langle \eta \rangle M'_\eta |^2 + G_2 | \langle \eta \rangle M'_{\eta'} |^2, \quad (49)$$

where

$$M'_\lambda = \sum_{i=1}^5 C_{\lambda i} M_i, \quad M'_\eta = \sum_{i=1}^5 C_{\eta i} M_i, \quad M'_{\eta'} = \sum_{i=6}^7 C'_{\eta' i} M_i. \quad (50)$$

We refer the coefficients  $C_{xi}$  and  $C'_{xi}$  to [41, 43]. The axial vector coupling constant  $g_A^4$  is included in the phase space factor  $G_i$ .

### C. Estimation of $N\Delta$ transition in $0\nu$ DBD

The hadron currents  $J_L^\mu$  and  $J_R^\mu$  are given in terms of current quarks. In the standard nuclear physics approach, the nuclear state vector is described using only nucleon degrees of freedom, instead of quarks. Therefore effective DBD interaction Hamiltonian has to be described by using nucleon degrees of freedom. This is achieved in two steps. At first, the semi-leptonic interaction is truncated into hadron degrees of freedom. The interaction Hamiltonian consists of nucleon current and  $N\Delta$  transition current and possible weak pion production current as shown in left panel of Fig. 1.

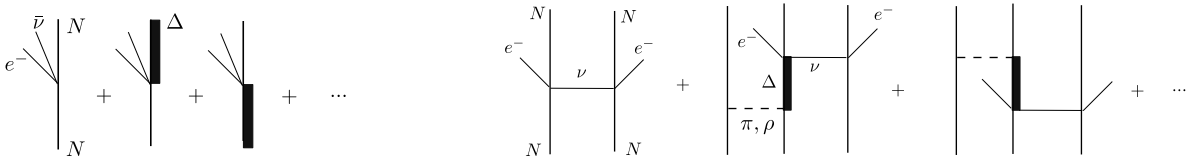


FIG. 1. Semileptonic interaction of hadron. Left panel shows electron and neutrino production processes of nucleon and  $N \leftrightarrow \Delta$  transition. Right panel shows 2N-mechanism of DBD.

In the second step, hadron degrees of freedom other than nucleon are eliminated and effective Hamiltonian to be used with many body wave function of nucleon is obtained. The resultant effective semileptonic Hamiltonian is well known for beta decay, muon capture and neutrino reaction. The nuclear weak current consists of one-nucleon impulse current (IMP) and many-body meson exchange current (MEC).

$$J^\mu(\mathbf{x}) = J_{IMP}^\mu(\mathbf{x}) + J_{MEC}^\mu(\mathbf{x}). \quad (51)$$

The contribution of  $\Delta$  appears as MEC. Basic mechanism of DBD due to nuclear weak current in Eq.(51) is the neutrino exchange between nucleons shown in the right panel of Fig. 1, which include IMP and MEC (2N-mechanism). The MEC of axial vector current contributes partly to the quenching of  $g_A$  seen in beta decay [12, 47]. Since the high momentum will be carried by exchanged neutrino in DBD compared with beta-decay and  $2\nu$  DBD,  $g_A^{eff}$  might depend on the kinematics of the process.

The  $\Delta$  mechanism which emerges in DBD is shown in left panel of Fig. 2 [1, 38]. Neutrino is exchanged between quarks within single hadron. This mechanism generates new MEC as shown in the right panel of Fig. 2. Among the excited nucleon states, resonance must be iso-spin 3/2  $\Delta$  resonance.  $\Delta_{33}(1232)$  is expected to give the largest contribution. Then  $N\Delta$  DBD contributes for  $0^+ \rightarrow 2^+$  transition( $\Delta$ -mechanism) but not for  $0^+ \rightarrow 0^+$  transition.

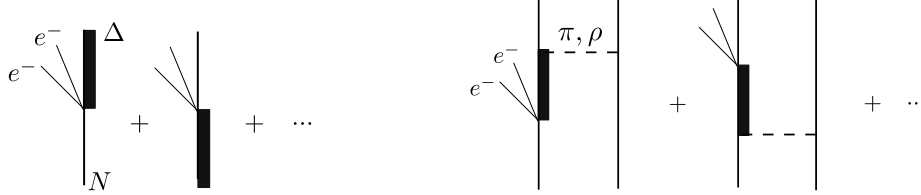


FIG. 2. Diagrams of neutrino exchange within baryon. Left panel shows  $0\nu$  DBD of  $N \leftrightarrow \Delta$  transition. Right panel shows  $\Delta$ -mechanism of DBD.

Within the non-relativistic constituent quark model with SU(6) symmetry, the matrix element of  $h_{AA}$  for  $n \rightarrow \Delta^{++}$  transition is given as

$$\mathcal{M}_\Delta = \langle \Delta^{++} || h_{AA} || n \rangle = \langle \Delta^{++} || \sum_{i,j=1}^3 \frac{2}{3} [\boldsymbol{\sigma}_i \otimes \boldsymbol{\sigma}_j]^{(2)} h(r_{ij}) || n \rangle = -\frac{8\sqrt{10}}{3} \langle h \rangle, \quad (52)$$

where the first term of  $h_{AA}$  in Eq. (46) in terms of quark operator contributes. The  $\Delta$ -mechanism contributes to both  $\eta$  and  $\lambda$  terms.

The  $\Delta$ -mechanism is estimated in Ref. [1]. They give a large contribution of the  $\Delta$  mechanism. It is estimated by using the probability of the  $\Delta$  in nuclear wave function  $P(\Delta)$  and the transition matrix element of the  $A-1$  nucleons  $\langle \Phi_F | \Phi_I \rangle$ .  $P(\Delta)$  is estimated as  $P(\Delta) \sim 0.01$  following Ref. [42] based on the probability of iso-spin 1/2  $N^*$  resonances instead of  $\Delta$ , suggested by the analysis of magnetic moment and  $(p, d)$  reaction at that time. The transition matrix element is assumed to be  $\langle \Phi_F | \Phi_I \rangle \sim \sqrt{0.1}$ . Using those numbers,  $\Delta$ -mechanism is estimated as,

$$\frac{\langle 2^+ || h_{AA} || 0^+ \rangle}{|\mathcal{M}_\Delta|} = \sqrt{P(\Delta)} \langle \Phi_F | \Phi_I \rangle \sim 3.2 \times 10^{-2}. \quad (53)$$

The  $\Delta$ -mechanism is studied in the microscopic model for the DBD of  $^{76}\text{Ge}$  in Ref. [41]. The  $\Delta$  component in nuclei is evaluated perturbatively by using the transition potential  $V_{NN \leftrightarrow N\Delta}$ ,

$$\langle 2^+ || h_{AA} || 0^+ \rangle = \langle F || V_{NN-N\Delta} \frac{1}{E_f - H} \langle \Delta | h_{AA} | N \rangle + \langle N | h_{AA} | \Delta \rangle \frac{1}{E_i - H} V_{N\Delta-NN} || I \rangle. \quad (54)$$

The  $NN-N\Delta$  transition potential is given by the pion and rho meson exchange model. The energy denominator is approximated by the  $N\Delta$  mass difference  $E_{i/f} - H \sim m_N - m_\Delta$ . The  $\Delta$ -mechanism is evaluated by the meson-exchange current in Fig. 2 with 'Hartree-Fock-Bogoliubov type' nuclear wave function. The  $\Delta$ -mechanism of the microscopic model turn out to be about 1/60 of the estimation of (53).

The dominant contribution of the  $\Delta$ -mechanism is due to the matrix element of the following operator:

$$\sum_{m,n=1}^A \tau_m^+ \tau_n^+ \boldsymbol{\sigma}_m \cdot \boldsymbol{\sigma}_n [\hat{r}_{mn} \otimes \hat{r}_{mn}]^{(2)}. \quad (55)$$

The ratio of the NME of operators which have the same spin and angular momentum structure for both the 2N- and  $\Delta$ -mechanism gives us less model dependent estimation of the  $\Delta$ -mechanism. Using the notation of Ref. [41],  $M_1$  is for the 2N-mechanism and  $M_9$  and  $M_{12}$  are for the  $\Delta$ -mechanism. Apart from coupling constants, difference among the matrix element  $M_i$  is only radial dependence of the operators, which is  $h(r)$  for 2N-mechanism while that

of the  $\Delta$ -mechanism with one-pion-exchange is  $Y_2(m_\pi r) = e^{-m_\pi r}(1 + 3/(m_\pi r) + 3/(m_\pi r)^2)/r$ . Using the numbers of Ref. [41], the ratio is calculated as

$$r = \frac{C_{\lambda 1} M_1}{c_9 M_9 + c_{12} M_{12}} \sim 0.12. \quad (56)$$

Assuming the  $A$ -dependence of the radial overlap integral is weak, the  $\Delta$ -mechanism for this particular type of matrix element is estimated as about 10% of that of the 2N-mechanism using  $g_A = 1.27$ , while the  $\Delta$ -mechanism can be 20% using quenched  $g_A^{eff} \approx 0.7$  [47].

#### IV. NUCLEAR AND DETECTOR SENSITIVITIES FOR DBD RHCS

##### A. The $\nu$ -mass and RHC sensitivities in DBD experiments

We discuss first individual DBD rates for the  $\nu$ -mass and RHC processes to see how the rates depend on  $\langle m \rangle$ ,  $\langle \lambda \rangle$  and  $\langle \eta \rangle$ . The DBD rate  $\Gamma_k$  with  $k$  being  $m, \lambda, \eta$  for the  $0^+ \rightarrow 0^+$  ground state transition is given as [15, 44]

$$\Gamma_k^{(0)} = (\langle k \rangle S_k(M_k G_k))^2, \quad S_k(M_k G_k) \approx M_k G_k^{1/2}, \quad (57)$$

where  $S_k(M_k G_k)$  is the sensitivity for the  $k$ -process ( $k : m, \lambda, \eta$ ) with  $M_k$  and  $G_k$  being the NME and the phase space factor. In this section,  $\langle m \rangle$  is given in units of  $m_e$ , i.e.  $\langle m \rangle = \langle m \rangle / m_e$ . The sensitivity is a kind of the amplification factor to make the small  $\langle k \rangle$  visible experimentally.  $M_k$  and  $G_k$  stand for the nuclear and atomic sensitivities, i.e. nuclear and atomic amplification factors. The axial-vector weak coupling factor of  $g_A^4$  with  $g_A$  being the axial-vector coupling for a free nucleon is included in  $G_k$ .

The NMEs are conventionally expressed as  $M_m = M_{GT}(1 + \chi_F + \chi_T)$  with  $\chi_F$  and  $\chi_T$  being the Fermi and tensor coefficients,  $M_\lambda = \chi_{2-}$ , and  $M_\eta = \chi'_R$ , and the phase space factors are  $G_m = G_{01}$ ,  $G_\lambda = G_{02}$ , and  $G_\eta = G_{09}$  [1]. In fact the sensitivity of  $S_\lambda$  includes higher order terms with  $G_{03}$  and  $G_{04}$ , which are of the order of a few % of the main term with  $G_{02}$ .

The phase space factor  $G_k$ , which depends on the DBD  $Q$  value and the atomic number, is evaluated theoretically. The RHC factors are found to be given by the mass one as

$$G_\lambda^{1/2} \approx 2 \times G_m^{1/2}, \quad G_\eta^{1/2} \approx 200 \times G_m^{1/2}, \quad (58)$$

The RHC sensitivities of  $S_\lambda$  and  $S_\eta$  depend linearly on the NMEs, which depend much on the nuclear models and nuclear parameters used for calculating them, as discussed in Sec. 1. The sensitivities are evaluated by using for examples the QRPA NMEs in [45] and [38] and the shell model NMEs in [43]. They are shown for typical DBD nuclei as a function of the mass number  $A$  in Fig. 3 and Fig. 4. Actually, the DBD nuclei shown here are all promising nuclei from experimental view points because of the large  $Q$  value, the large natural isotope abundance, the good energy-resolution, and thus the ton-scale DBD plans are under progress or consideration [6, 7].

The RHC sensitivities of  $S_\lambda$  and  $S_\eta$  are found to be around  $10^{-6}$  and  $10^{-10}$ , respectively, and increase as the  $\nu$ -mass one of  $S_m$  increases as

$$S_\lambda \approx a_\lambda \times S_m, \quad S_\eta \approx a_\eta \times S_m, \quad (59)$$

with  $a_\lambda \approx 1-2$  and  $a_\eta \approx 200$ . These are similar as the phase space factors in Eq. (58), suggesting similar NMEs of  $M_\lambda \approx M_\eta$ . Actually, many multipole states with  $J=0-7$  over an wide excitation region of  $E=0-15$  MeV in the intermediate nucleus are involved in DBD, and thus  $M$  reflects gross features of the nucleus, being rather insensitive to the valence nucleon configuration of the individual nucleus, as given by the simple relation of  $M_m = 5.2-0.023 A$  with  $A$  being the mass number [47]. Here the key nuclear parameter of the effective coupling of  $g_A^{eff}/g_A \approx 0.65$  is used. Then a similar relation may be expected also for  $M_\lambda$  and  $M_\eta$ , and thus experimental studies on several DBD nuclei (detectors) are useful to check and confirm the RHC signals.

The sensitivities for  $\langle \eta \rangle$  are larger by a factor around 200 than those for the  $\langle m \rangle$  and  $\langle \lambda \rangle$ , reflecting the same factor as the square root of the phase space factors. This indicates that the relative NMEs for  $\nu$ -mass and RHCs are nearly same. The RHC sensitivities are nearly proportional to the  $\nu$ -mass sensitivity as shown in Fig. 4, reflecting the RHC phase space factors proportional to the  $\nu$ -mass one.

The  $\nu$ -mass of  $\langle m \rangle$  and the RHCs of  $\langle \lambda \rangle$  and  $\langle \eta \rangle$  to be studied are beyond the standard model, and thus are considered to be very small. No signals in  $0\nu$  DBD experiments so far suggest that the RHCs are as small as



$\langle \lambda \rangle \approx 10^{-7}$ , and  $\langle \eta \rangle \approx 10^{-9}$  or less. Accordingly the RHC DBD rate to be considered is of the order of  $10^{-35}$  per sec or less. This corresponds to a few DBD signals per 1 ton of the DBD isotopes per year. Thus it is studied by using ton-scale DBD isotopes for years. Then for practical use, we use as the DBD rate the signal rate per ton year (t y). It is expressed as

$$\Gamma_k = \left(\frac{\langle k \rangle}{k_0}\right)^2, \quad k_0 = \frac{0.15 \times 10^{-14} A^{1/2}}{S_k(M_k, G_k)}, \quad (60)$$

where  $k_0$  with  $k = m, \lambda, \eta$  stands for the unit effective  $\nu$ -mass (in units of  $m_e$ ) and the unit effective RHCs that give the rate of  $\Gamma_k=1$  per ton year. Actually,  $k_0$  is around  $1.5 \times 10^{-14}/S_k(M_k, G_k)$  for typical DBD nuclei of  $A \approx 100$  of the current interest.

Note that the transition rate per year is given as  $\ln 2 (T_{1/2})^{-1}$ , and thus the rate per t y is

$$\Gamma = (41.5/A)10^{28}(T_{1/2})^{-1} \quad (61)$$

with  $A$  being the mass number. Then, the rate of  $\Gamma=1$  per t y corresponds to the half-life of 0.55 for  $^{76}\text{Ge}$ , 0.42 for  $^{100}\text{Mo}$  and 0.31 for  $^{136}\text{Xe}$ , all in units of  $10^{28}$  years. Thus ton-scale DBD detectors are used to study RHC DBDs with half-life in the  $10^{27-28}$  y region.

Now we discuss the DBD transition to the  $2^+$  excited state. The DBD rate for the  $\nu$ -mass is reduced much for the  $2^+$  state, and thus the rate is given exclusively by the RHC terms. The transition rate  $\Gamma_k^{(2)}$  with  $k = \lambda, \eta$  is given by

$$\Gamma_k^{(2)} = (\langle k \rangle S'_k)^2, \quad (62)$$

where  $S'_k$  is the sensitivity for the  $k$ -process DBD to the  $2^+$  state. The sensitivities for  $\lambda$  and  $\eta$  are expressed as

$$S'_\lambda = M'_\lambda(G_1)^{1/2}, \quad S'_\eta = ((M'_\eta)^2 G_1 + (M'_{\eta'})^2 G_2)^{1/2}, \quad (63)$$

where  $M'_{k'}$  and  $G_1, G_2$  are the NMEs and the phase space factors for the  $k$ -process DBD. Here and hereafter dash indicates for the value of  $2^+$  transition as given in Eq. (50).

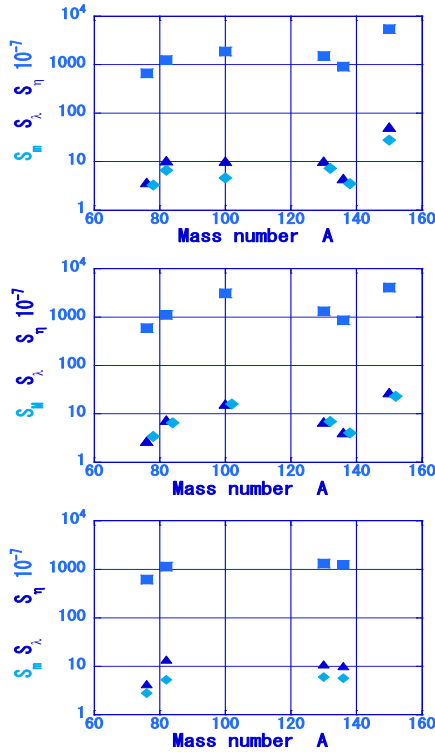


FIG. 3. DBD  $\nu$ -mass and RHC sensitivities.  $S_m$  (light blue diamond),  $S_\lambda$  (blue triangle) and  $S_\eta$  (blue square) for typical DBD nuclei of  $^{76}\text{Ge}$ ,  $^{82}\text{Se}$ ,  $^{96}\text{Zr}$ ,  $^{100}\text{Mo}$ ,  $^{116}\text{Cd}$ ,  $^{130}\text{Te}$ ,  $^{136}\text{Xe}$  and  $^{150}\text{Nd}$  of current interest. Top: QRPA NMEs in [45]. Middle: QRPA NMEs in [38]. Bottom: Shell model NMEs in [46]. Some  $S_m$  points are shifted by the mass number 2 to avoid overlap with the  $S_\lambda$  ones.

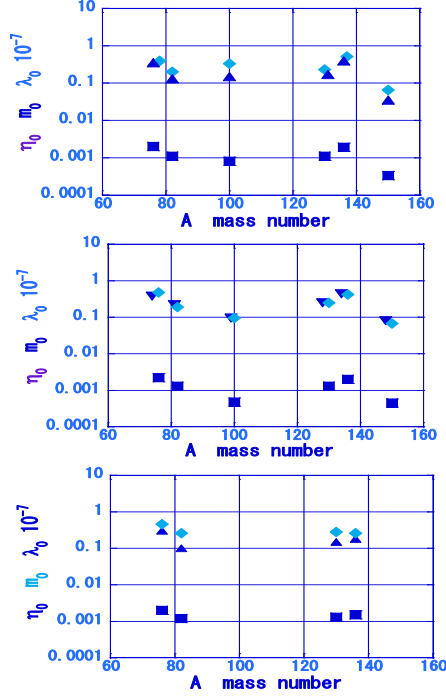


FIG. 4. The unit  $\nu$ -mass of  $m_0$  (light blue diamond) and the unit RHCs of  $\lambda_0$  (blue triangle) and  $\eta_0$  (blue square) for typical DBD nuclei of  $^{76}\text{Ge}$ ,  $^{82}\text{Se}$ ,  $^{96}\text{Zr}$ ,  $^{100}\text{Mo}$ ,  $^{116}\text{Cd}$ ,  $^{130}\text{Te}$ ,  $^{136}\text{Xe}$  and  $^{150}\text{Nd}$ . Top: QRPA NMEs in [45]. Middle: QRPA NMEs in [38]. Bottom: Shell model NMEs in [43]. Some  $m_0$  points are shifted by the mass number 2 to avoid overlap with the  $\lambda_0$  ones.

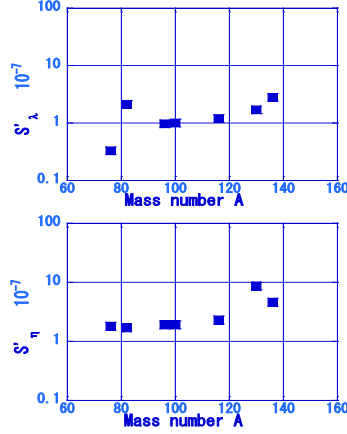


FIG. 5. RHC sensitivities of  $S'_\lambda$  (top) and  $S'_\eta$  (bottom) for the  $2^+$  state in the typical DBD nuclei of  $^{76}\text{Ge}$ ,  $^{82}\text{Se}$ ,  $^{100}\text{Mo}$ ,  $^{116}\text{Cd}$ ,  $^{130}\text{Te}$  and  $^{136}\text{Xe}$  of current interest. The NMEs used are in [43]

The phase space factors are found to be expressed as  $(G_2)^{1/2} \approx 0.8(G_1)^{1/2}$ . It is interesting to note that  $(G_1)^{1/2}$  and  $(G_2)^{1/2}$  for the excited states are nearly the same as  $G_m$  and  $G_\lambda$  for the ground states even though the  $Q$  value for the excited state is 20-30% smaller than that for the ground state. The sensitivities of  $S'_\lambda$  and  $S'_\eta$  for the excited state DBDs are shown in Fig. 5.

It is noted that the sensitivities of  $S'_\lambda$  and  $S'_\eta$  do not follow the trend of the phase space factors of  $G_1$  and  $G_2$  because the NME fluctuates much as the mass number (nucleus) changes. The sensitivity  $S'_\lambda$  is around  $1\text{-}3 \times 10^{-7}$  except  $0.3 \times 10^{-7}$  for  $^{76}\text{Ge}$ . This is about 1/3 of the  $S_\lambda$  for the ground state. This is mainly due to the smaller  $M'_\lambda$  by a factor 3 than  $M_\lambda$  for the ground state. The sensitivity  $S'_\eta$  is around  $2 \times 10^{-7}$  except  $7 \times 10^{-7}$  for  $^{130}\text{Te}$ . This is 2-3 orders of magnitude smaller than the one for the ground state because the phase space factors for the  $2^+$  state is 5

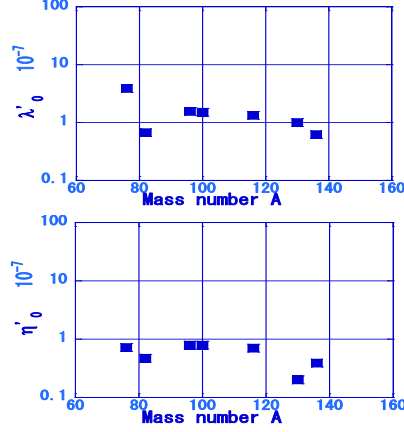


FIG. 6. The unit RHCs of  $\langle \lambda'_0 \rangle$  (top) and  $\langle \eta'_0 \rangle$  (bottom) for the excited state in the typical DBD nuclei of  $^{76}\text{Ge}$ ,  $^{82}\text{Se}$ ,  $^{100}\text{Mo}$ ,  $^{116}\text{Cd}$ ,  $^{130}\text{Te}$  and  $^{136}\text{Xe}$  of current interest. The NMEs used are in [43]

orders of magnitude smaller than  $G_{09}$  for the ground state. Then, the  $\eta$ -RHC is studied exclusively by measuring the ground state DBD [23], while the  $\lambda$ -RHC may be studied by measuring the excited state DBD as well as the ground state DBD.

The unit RHCs for the excited state are shown in Fig. 6. They correspond to the RHCs to be measured by a typical DBD detector with  $N=1$  ton  $B=1/\text{t y}$  and  $T=5$  y run.

### B. RHCs to be studied by ton-scale detectors

Experimentally, the  $\nu$ -mass and the RHCs to be measured depend on DBD detector specifications. The minimum  $\langle k \rangle$  to be measured by using a detector with  $N$  ton DBD isotopes for  $T$  years run is expressed as [15, 44]

$$k_m = d \times k_0, \quad d = 1.3 \times \epsilon^{-1/2} (B/NT)^{1/4}, \quad (64)$$

where  $k_m$  with  $k$  being  $m, \lambda, \eta$  is the minimum  $\langle k \rangle$  to be measured and  $d$  stands for the detector sensitivity. It is expressed by using the detector efficiency  $\epsilon$ , the background rate  $B$  per t y and the total DBD isotope mass  $N$  (ton). Since  $d$  depends on  $B^{1/4}$  and  $N^{-1/4}$ , one needs to reduce the BG rate ( $B$ ) and increase the total amount ( $N$ ) of the DBD isotopes by 2 orders of magnitude to reduce the minimum  $k$  to be measured by a factor 10 to go down from the IH  $\nu$ -mass region of  $\langle m_m \rangle \approx 30$  meV to the NH one of 3 meV.

We first discuss  $\langle k_m \rangle$  for the  $0^+$  ground state DBD. In case of a typical high-sensitivity DBD detector with  $N=1$  t,  $B=1/\text{t y}$ ,  $\epsilon=0.75$ , and  $T=5$  y, the detector sensitivity is  $d \approx 1$ . Then one gets  $k_m \approx k_0 = 0.15 \times 10^{-14} A^{1/2} / S_k$  with  $k = m, \lambda, \eta$ . In this case, the minimum  $\nu$ -mass of  $m_m$  and the minimum RHCs of  $\lambda_m$  and  $\eta_m$  are nearly the same as the  $m_0, \lambda_0, \eta_0$ .

It is interesting to note that the ratios of the minimum RHCs to the minimum  $\nu$ -mass are given approximately by the ratios of the phase space factors as

$$\frac{\lambda_m}{m_m} = \frac{\lambda_0}{m_0} \approx 1, \quad \frac{\eta_m}{m_m} = \frac{\eta_0}{m_0} \approx \frac{1}{200}. \quad (65)$$

Detectors for the IH  $\nu$ -mass of around  $m_m = 0.5 \times 10^{-7}$  ( $\langle m \rangle \approx 25$  meV) are used to search for the RHCs of  $\lambda \approx 0.5 \times 10^{-7}$  and  $\eta \approx 0.25 \times 10^{-9}$ .

The minimum RHC to be measured by the  $2^+$  excited state DBD is given as in case of the ground state DBD,

$$k'_m = d' \times k'_0, \quad d' = 1.3 \times \epsilon'^{-1/2} (B'/NT)^{1/4}, \quad (66)$$

where  $d'$  is the detector sensitivity for the  $2^+$  state. Here the DBD isotope mass  $N$  and the run time  $T$  for the excited state are same as those for the ground state. The  $B$  and  $B'$  are also same for simple calorimetric detectors to measure the summed energies of the two  $\beta$ -rays.

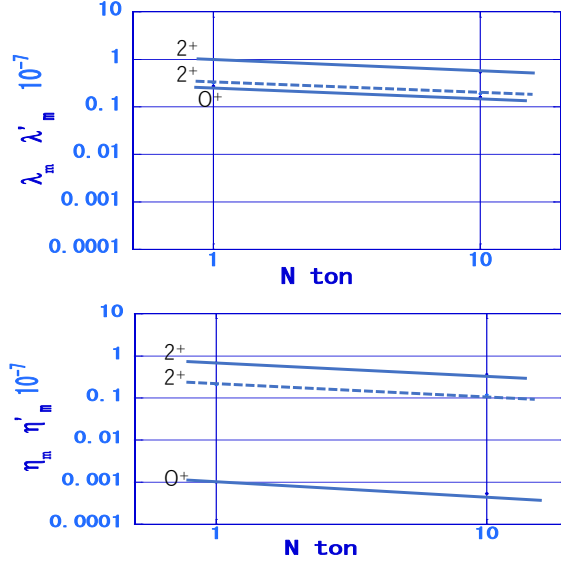


FIG. 7. The minimum RHCs to be measured as a function of  $N$  (DBD isotope mass in units of ton) for typical DBD nuclei (see caption 3). Solid lines for the ground and excited states with  $B=1$  and  $B'=1$ . Dashed lines for the excited state with  $B'=0.01$  by the  $\gamma$  coincidence measurement. Top panel:  $\lambda_m$  for the  $0^+$  ground state and  $\lambda'_m$  for the excited  $2^+$  state. Bottom panel:  $\eta_m$  for the  $0^+$  ground state and  $\eta'_m$  for the excited  $2^+$  state.

The present work emphasizes measurement of the  $\gamma$  ray from the  $2^+$  state as well as the  $\beta\beta$  rays to the  $2^+$  state. Using the  $Q$  values of  $Q$  and  $Q'$  for the ground and excited state DBDs, the  $\beta\beta$  energies for them are  $E_{\beta\beta} = Q$  and  $E'_{\beta\beta} = Q'$  and the energy of the  $\gamma$  ray from the excited state is  $E_\gamma = Q - Q'$ . Then the  $2^+$  state DBD is measured by observing the total energy of  $E'_{\beta\beta} + E_\gamma = Q$  in coincidence the  $\gamma$  signal with  $E_\gamma = Q - Q'$  to separate the transition from the ground state transition and to reduce substantially backgrounds associated with RI impurities. The background contribution from the  $2\nu$  DBD decay to the excited state is also much smaller by a factor around  $(Q'/Q)^5 \approx 0.1$  than that for the ground state transition. Back grounds from solar neutrinos are also reduced much [48, 49]. Actually, the background reduction rate depends much on the energy resolution of the  $\gamma$  measurement. It is of the order of  $B'/B \approx 0.01$  in case of bolometers with the energy resolution of 10 keV. Then the minimum RHCs to be measured by the  $2^+$  DBD get smaller by a factor around  $(0.01)^{1/4} \approx 0.3$  by requiring coincidence with the  $\gamma$  ray.

The minimum RHCs of  $k_m$  and  $k'_m$  are evaluated in cases of  $B=1$  and  $B'=1$  and 0.01 as a function of  $N$  for typical DBD nuclei as shown in Fig. 7. Here the unit RHCs are assumed to be  $\lambda_0 = 0.27, \eta_0 = 0.001$  for the ground state and  $\lambda'_0 = 1, \eta'_0 = 0.7$ , all in units of  $10^{-7}$ , as shown in Fig. 4 and Fig. 6.

The  $\eta$  current of the order of  $\langle \eta \rangle \approx 10^{-10}$  will be observed in the ground state transition, but not in the excited state transition. On the other hand  $\lambda_m$  for the ground state transition with  $B=1$  is nearly same as  $\lambda'_m$  for the excited state with  $B' = 0.01$ , and thus the  $\lambda$  current of the order of  $\langle \lambda \rangle \approx 3 \times 10^{-7}$  will be observed in both the  $0^+$  ground state and  $2^+$  excited state transitions.

Let us discuss realistic cases where both the  $\lambda$  and  $\eta$  currents coexist as given in Eqs. (11) and (49). For simplicity, we discuss the RHCs in the case of the NH mass spectrum, where  $\langle m \rangle \approx 7 \times 10^{-9}$  (3.5 meV). Then the RHCs to be studied by ton-scale experiments with  $B$  and  $B'$  being around 1/t y and 0.01/t y are of the orders of  $10^{-7}$  for  $\langle \lambda \rangle$  and  $10^{-10}$  for  $\langle \eta \rangle$ . In these regions, the contribution from the mass term is much smaller than those from the RHC ones. Then the minimum RHCs to be studied are given by ellipsoids in Fig. 8 for  $^{76}\text{Ge}$  and in Fig. 9 for  $^{136}\text{Xe}$ .

The minimum RHCs of  $\langle \lambda_m \rangle$  and  $\langle \eta_m \rangle$  to be measured are around  $0.3 \times 10^{-7}$  and  $0.2 \times 10^{-9}$  for the  $0^+$  ground state DBDs of  $^{76}\text{Ge}$  and  $^{136}\text{Xe}$ , while the minimum  $\langle \lambda'_m \rangle$  is around  $1 \times 10^{-7}$  and  $0.5 \times 10^{-7}$  for the  $2^+$  excited state DBDs of  $^{76}\text{Ge}$  and  $^{136}\text{Xe}$ . The small  $\langle \lambda' \rangle$  for the  $^{136}\text{Xe}$   $2^+$  state is due to the large NME of  $M'_\lambda$ .

So far we have discussed the  $\nu$ -mass and the RHCs to be studied on the basis of the model NMEs with the weak coupling of  $g_A$  for a free nucleon. Actually, the NMEs are sensitive to nuclear and non-nuclear spin( $\sigma$ )-isospin( $\tau$ ) correlations and nuclear medium effects. Then the real GT(Gamow-Teller) NMEs are reduced (quenched) much than the model NMEs without these effects. Then effective coupling constant of  $g_A^{eff}$  is introduced in order to incorporate the effects which are not properly included in the model calculation. Actually the RHC NMEs in [43] are calculated for the quenched  $g_A$  by 0.75 as well. The quenching coefficient,  $g_A^{eff}/g_A$  has been recently shown to be around 0.65 in case of the QRPA model [13, 15, 47].

The axial-vector components in the  $M_m$  and  $M_\lambda$  are quenched by the factor  $(g_A^{eff}/g_A)^2 \approx 0.4$ , and thus  $M_m$  and

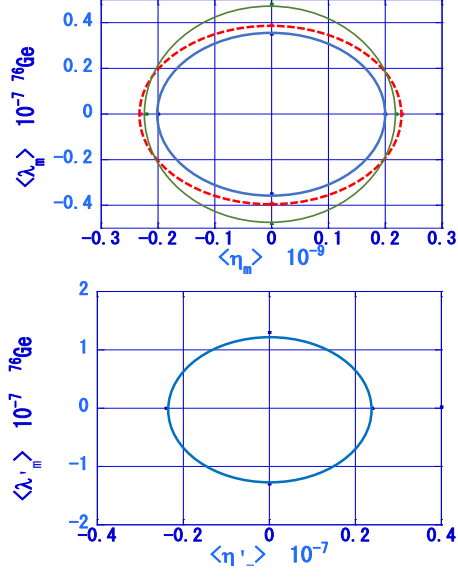


FIG. 8. The minimum RHCs to be measured by the  $^{76}\text{Ge}$ . Top panel: The  $0^+$  ground state transition with the detector sensitivity of  $d=1$ . The NMEs  $M_\lambda$  are the QRPA ones by [45] (thick blue line), [33] (dotted red line), [38] (thin green line). Bottom panel: The  $2^+$  excited state transition with the detector sensitivity of  $d=0.01$  and the NMEs of QRPA in [43]

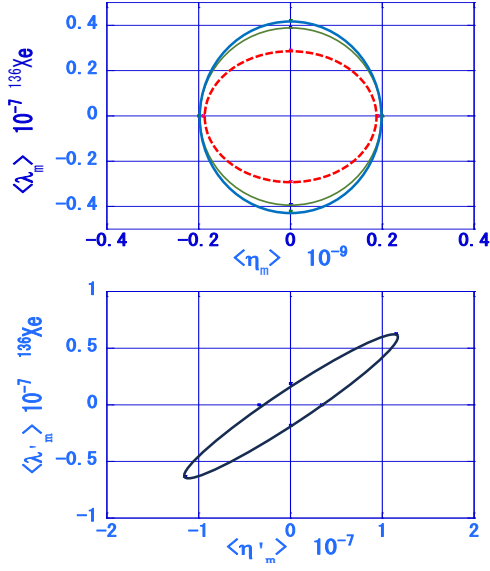


FIG. 9. The minimum RHCs to be measured by the  $^{136}\text{Xe}$ . See caption of Fig. 8. Note the large interference terms of  $\langle \lambda \rangle$  and  $\langle \eta \rangle$  in the  $2^+$  transition.

$M_\lambda$  are reduced by a factor around 0.5-0.6, depending on the vector components, while  $M_\eta$  is reduced by the factor  $g_A^{eff}/g_A \approx 0.6$ . Accordingly the actual RHCs to be studied are about a factor 2 larger than the RHCs given in Fig. 7, i.e.  $\langle \eta \rangle \approx 2 \times 10^{-10}$  and  $\langle \lambda \rangle \approx 5 \times 10^{-8}$  by using DBD detectors with  $N = 1, B = 1, B' = 0.01$ . The limits get smaller by 20 % by using larger DBD isotope-mass  $N$  or less background  $B$  detector by a factor 2.

The RHCs of  $\langle \lambda \rangle$ ,  $\langle \eta \rangle$  and  $\tan\beta$  to be studied or constrained by the ton-class DBD experiment for both the ground  $0^+$  and  $2^+$  transitions are as given below. Here we assume the NH mass spectrum.

- A:  $M_\lambda \ll M'_\lambda$  and the  $0\nu\beta\beta$  signal in  $2^+$ , but not in  $0^+$ .  $|\langle \lambda \rangle| \approx 5 \times 10^{-8}, |\langle \eta \rangle| \leq 2 \times 10^{-10}, 1/\xi \geq 2.5 \times 10^2$ .
- B: The  $0\nu\beta\beta$  signal in  $2^+$  and  $0^+$ .  $|\langle \lambda \rangle| \approx 5 \times 10^{-8}, |\langle \eta \rangle| \approx 2 \times 10^{-10}, 1/\xi \approx 2.5 \times 10^2$ .
- C: The  $0\nu\beta\beta$  signal in  $0^+$ , but not in  $2^+$ .  $|\langle \lambda \rangle| \leq 5 \times 10^{-8}, |\langle \eta \rangle| \approx 2 \times 10^{-10}, 1/\xi \leq 2.5 \times 10^2$ .

The cases of A and B with non-zero  $0\nu\beta\beta$  signals in the  $2^+$  decay, are unlikely if  $1/\xi \approx \tan\beta$  from (21) and (26). In other words, the observation of the  $0\nu$  DBD events in the  $2^+$  channel indicates  $1/\xi \gg 500$ .

So far we have discussed the DBD rate based on the QRPA model NMEs. In fact there are several ways (models) to evaluate the DBD NMEs, and the evaluated NMEs scatter over an order of magnitude, depending on the models [15]. Recent IBM (Interacting Boson Model) NMEs [50] for the  $2^+$  RHCs are smaller by an order of magnitude than the QRPA ones. These smaller NMEs give the minimum  $\langle \lambda' \rangle_m$  around  $3 \times 10^{-6}$  in case of  $N = 1, B' = 0.01/t$  y, which is larger than the value with the QRPA NME by an order of magnitude. Then one can not expect any neutrinoless signal in the  $2^+$  transition, but only in the  $0^+$  transition in case of  $\langle \lambda \rangle \approx 3 \times 10^{-7}$  and/or  $\langle \eta \rangle \approx 10^{-10}$ . In this case one has to measure the energies of individual  $\beta$  rays to identify experimentally the RHC to be  $\langle \lambda \rangle$  or  $\langle \eta \rangle$  once the  $0\nu\beta\beta$  signal is observed, although it likely be due to  $\langle \eta \rangle$  if we assume (21) and if  $\tan\beta \leq 60$ .

## V. CONCLUDING REMARKS

In the present paper, we have studied in the framework of the  $L - R$  symmetric model the NMEs and the  $\langle \lambda \rangle$  and  $\langle \eta \rangle$  terms to be studied in the next-generation ton-scale DBD detectors. They are as given below.

1. Ton-scale DBD detectors are under construction to explore DBDs in the new region of  $T_{1/2} \approx 10^{27-28}$  y of current interest to search for the effective  $\nu$ -mass in the IH region around 15-45 meV. The  $\nu$ -mass spectrum, however, is likely be NH on the basis of the theoretical considerations and the experimental limit on the sum of the  $\nu$ -masses in the universe. Then the effective NH mass gets smaller by an order of magnitude than the IH mass, and the half-life smaller by 2 orders of magnitude. Then one may expect almost no contributions from the  $\nu$ -mass terms, and thus we may study well the RHCs in the interesting region which have not been measured.

2. By examining  $0^+$  and  $2^+$  transitions, we have explored both  $\langle \lambda \rangle$ - and  $\langle \eta \rangle$ -terms in the NH case. Their values depend on NMEs and phase space volumes.

3. The NMEs involved in the RHCs have been explicitly given from a simple derivation for both the  $0^+$  and the  $2^+$  transitions. The enhancement mechanism of the  $\langle \eta \rangle$ -term for the  $0^+$  transition has been discussed. The  $\Delta$ -mechanism, where  $\nu$  exchange between quarks, appears for the  $2^+$  transition. Guided by the analysis of the  $^{76}\text{Ge}$  DBD, the  $\Delta$  mechanism is estimated about 10% or 20% of the  $2N$ -mechanism for the leading axial vector current NME of  $\sigma_m \cdot \sigma_n Y_2$  depending on the  $g_A$  of free nucleon or the quenched  $g_A^{eff}$ .

4. The RHC DBD rate to be observed by the ton-scale experiment with  $N=1$  ton isotopes and BG rate of  $B=1$  per ton year and  $T=5$  year run is around  $\Gamma=1/\text{ton year}$ , which corresponds to the half-life around  $(40/A) 10^{28}$  years with  $A$  being the mass number.

5. The RHCs to be observed by the ton-scale DBD detector are  $|\langle \lambda \rangle| \approx 8 \times 10^{-8}$  and  $|\langle \eta \rangle| \approx 4 \times 10^{-10}$ , depending on the NMEs. They are studied by measuring the  $0^+$  ground state transition, while only the  $\lambda$ -current is studied by measuring the excited  $2^+$  transition in coincidence with the  $\gamma$ -ray from the  $2^+$  state to the ground state. Here the smaller phase-space factors for the excited state is compensated by the lower BG rate of  $B \approx 0.01$  in the  $\gamma$ -ray coincidence measurement.

6. The studies of both the ground and excited state DBDs are used to get the RHCs or the limits on them, and  $\tan\beta$ , the ratio of them, which are of interest from particle physics models. Needless to say, a number of ton-scale low-BG detectors are useful to confirm the ultra-rare RHC signals among background ones.

7. The DBD rate is given in terms of the products of the RHC  $\langle k \rangle$  and NME  $M_k$  with  $k = \lambda, \eta$  and the NME depends much on the nuclear model and the nuclear parameters used for the model, it is valuable to study them on several nuclei to confirm the RHC. It is highly appreciated to evaluate accurate values for the NMEs involved in the RHCS. In principle, precise measurements of RHCs in 2 nuclei would give  $\langle \lambda \rangle$  and  $\langle \eta \rangle$ , provided that the accurate values for the NMEs would be well known. Then, once the RHC signals are identified, measurements of energy and angular correlations of the individual  $\beta$  rays by using tracking detectors are encouraged to identify the RHC as  $\langle \lambda \rangle$  or  $\langle \eta \rangle$  or both.

## VI. ACKNOWLEDGMENTS

This work was partly supported by JSPS KAKENHI Grants No. 23K22508 (T.F.).

---

[1] M. Doi, T. Kotani, and E. Takasugi, Double Beta Decays and Majorana Neutrino, Prog. Theor. Phys. Suppl. **83**, 1 (1985).  
 [2] H. Ejiri, Double beta decays and  $\nu$  masses. J. Phys. Soc. Jpn. **74**, 2101(2005).

- [3] F. Avignone, S. Elliott, and J. Engel, Double beta decay, Majorana  $\nu$ , and  $\nu$  mass. *Rev. Mod. Phys.* **80**, 481 (2008).
- [4] H. Ejiri, Double  $\beta$ -decays and  $\nu$  nuclear responses. *Prog. Part. Nucl. Phys.* **54**, 249 (2010).
- [5] J. Vergados, H. Ejiri, and F. Šimkovic, Theory of neutrinoless double- $\beta$ -decay. *Rep. Prog. Phys.* **75**, 106301 (2012).
- [6] M. Agostini, G. Benato, J. A. Detwiler, J. Menéndez, and F. Vissani, Toward the discovery of mattercreation with neutrinoless  $\beta\beta$  decay, *Rev. mod. Phys.* **95** 025002.
- [7] S. Umehara and H. Ejiri, Neutrino masses and right-handed weak currents studied by neutrino-less  $\beta\beta$ -decay detectors, *Universe* **10**, 247 (2024).
- [8] J. Suhonen and O. Civitarese, Weak interaction and nuclear structure aspect of nuclear double beta decay. *Phys. Rep.* **300**, 123 (1998).
- [9] A. Faessler and F. Simkovic, Double beta decay. *J. Phys. G Nucl. Part. Phys.* **24**, 2139 (1998).
- [10] J. Suhonen and O. Civitarese, Double-beta decay nuclear matrix elements in the pnQRPA framework. *J. Phys. G Nucl. Part Phys.* **39**, 085105 (2012).
- [11] J. Engel and J. Menéndez, Status and future of nuclear matrix elements for  $\nu$ less double  $\beta$ -decay: A review. *Rep. Prog. Phys.* **80**, 046301 (2017).
- [12] H. Ejiri, Nuclear matrix elements for  $\beta$  and  $\beta\beta$  decays and quenching of the weak coupling  $g_A$  in QRPA. *Front. Phys* **7**, 30 (2019).
- [13] H. Ejiri, Nuclear spin isospin responses for low-energy  $\nu$ s. *Phys. Rep.* **338**, 265 (2000)
- [14] J. Suhonen, J. Impact of the quenching of  $g_A$  on the sensitivity of  $0\nu\beta\beta$  experiments. *Phys. Rev. C* **96**, 055501 (2017).
- [15] H. Ejiri, J. Suhonen and K. Zuber,  $\nu$  nuclear responses for astro- $\nu$ s, single  $\beta$ -decays, and double  $\beta$ -decays. *Phys. Rep.* **797**, 1 (2019).
- [16] T. Fukuyama, K. Ichikawa, and Y. Mimura, Revisiting fermion mass and mixing fits in the minimal SUSY SO(10) GUT, *Phys. Rev. D* **94**, 075018 (2016).
- [17] A. G. Adame et al., (DESI Collaboration) , DESI 2024 VI: Cosmological Constraints from the Measurements of Baryon Acoustic Oscillations, arXiv:2404.03002.
- [18] N. Aghanim et al., (Planck Collaboration), Planck 2018 results. V. CMB power spectra and likelihoods, *Astron. Astrophys.* **641**, A5 (2020), arXiv:1907.12875.
- [19] F.J. Qu et al., (ACT Collaboration), The Atacama Cosmology Telescope: A Measurement of the DR6 CMB Lensing Power Spectrum and its Implications for Structure Growth, *Astrophys. J.* **962**, no. 2 112 (2024), arXiv:2304.05202.
- [20] M. Sen and A.Y. Smirnov, Neutrinos with refractive masses and the DESI BAO results, arXiv:2407.02462.
- [21] H. Ejiri, N. Kamikubota, Y. Nagai, T. Nakamura, K. Okada T. Shibata et al., Double Beta Decay of  $^{76}\text{Ge}(0^+) \rightarrow 0^+$  and  $2^+$  States in  $^{76}\text{Se}$  Studied by the  $\beta - \gamma$  Coincidence Method, *Journal of Physics G: Nuclear Physics* **13**, 839, (1987).
- [22] H. Ejiri, K. Fushimi, K. Hayashi, R. Hazama, T. Kishimoto, N. Kudomi et al., Limits on neutrinoless double beta decay of Mo-100, *Nucl. Phys. A* **611**, 85, (1996).
- [23] T. Fukuyama and T. Sato, Neutrinoless double beta decay and  $\langle \eta \rangle$  mechanism in the left-right symmetric model, *JHEP* **06**, 049 (2023).
- [24] P. Minkowski,  $\mu \rightarrow e\gamma$  at a Rate of One Out of  $10^9$  Muon Decays ?, *Phys. Lett.* **B67**, 421 (1977).
- [25] T. Yanagida, Horizontal gauge symmetry and masses of neutrinos, *Conf. Proc.* **C7902131**, 95 (1979).
- [26] M. Gell-Mann, P. Ramond, and R. Slansky, Complex Spinors and Unified Theories, *Conf. Proc.* **C790927**, 315 (1979).
- [27] R. N. Mohapatra and G. Senjanovic, Neutrino Mass and Spontaneous Parity Nonconservation, *Phys. Rev. Lett.* **44**, 912 (1980).
- [28] J. Kersten and A.Y. Smirnov, Right-Handed Neutrinos at CERN LHC and the Mechanism of Neutrino Mass Generation, *Phys. Rev. D* **76**, 073005 (2007).
- [29] C.H. Lee, P.S. Bhupal Dev, and R.N. Mohapatra, Natural TeV-scale left-right seesaw mechanism for neutrinos and experimental tests, *Phys. Rev. D* **88**, 093010 (2013).
- [30] F. Simkovic, J. Vergados, and A. Faessler, Few active mechanisms of the neutrinoless double beta-decay and effective mass of Majorana neutrinos, *Phys. Rev. D* **82**, 113015 (2010).
- [31] J. Engel and J. Menendez, Status and future of nuclear matrix elements for neutrinoless double-beta decay: a review, *Rep. Prog. Phys.* **80** 046301 (2017).
- [32] G. Pantis, A. Faessler, W.A. Kaminski, and J.D. Vergados, Description of the 0 neutrino beta decay of  $^{48}\text{Ca}$ ,  $^{76}\text{Ge}$ ,  $^{100}\text{Mo}$ ,  $^{128}\text{Te}$ ,  $^{130}\text{Te}$ , *J. Phys. G: Nucl. Phys.* **18**, 605 (1992).
- [33] G. Pantis, F.Simkovic, J.D. Vergados, and A. Faessler, Neutrinoless double beta decay within QRPA with proton-neutron pairing, *Phys. Rev. C* **53**, 695 (1996).
- [34] J. Suhonen and O. Civitarese, Weak-interaction and nuclear-structure aspects of nuclear double beta decay, *Phys. Rep.* **300**, 123 (1998).
- [35] Y. Zhang, H. An, X. Ji, and R.N. Mohapatra, General CP Violation in Minimal Left-Right Symmetric Model and Constraints on the Right-Handed Scale, *Nucl. Phys.* **B802**, 247 (2008).
- [36] For a review, P. Langacker, *The Standard Model and Beyond* (CRC Press 2009).
- [37] A.M. Sirunyan et al. (CMS Collaboration), Search for W' bosons decaying to a top and a bottom quark at s=13TeV in the hadronic final state, *Phys. Lett.* **B820**, 136535 (2021).
- [38] T. Tomoda, Double beta decay, *Rep.Prog.Phys.* **54**, 53 (1991).
- [39] T. Tomoda, A. Faessler, K. W. Schmid and F. Grümmer, NEUTRINOLESS DOUBLE BETA DECAY AND A NEW LIMIT ON THE LEPTON NUMBER VIOLATION, *Phys. Lett.* **157B**, 4 (1985).
- [40] W. Horiuchi, T. Sato, Y. Uesaka and K. Yoshida, Electron wave functions in beta-decay formulas revisited (I): Gamow-Teller and spin-dipole contributions to allowed and first-forbidden transitions, *PTEP* **2021**, 103D03 (2021).

- [41] T. Tomoda,  $0^+ \rightarrow 2^+$  Neutrinoless Beta Beta Decay of  $^{76}\text{Ge}$ , Nucl. Phys. **A484**, 635 (1988).
- [42] H. Primakoff and S.P. Rosen, Nuclear double-beta decay and a new limit on lepton nonconservation, Phys. Rev. **107**, 1925 (1969).
- [43] D.L. Fang and A. Faessler,  $0\nu\beta\beta$  decay to the first  $2^+$  state with a two-nucleon mechanism for a  $L - R$  symmetric model, Phys.Rev. **107**, 015501 (2023).
- [44] H. Ejiri,  $\nu$ -mass sensitivity and nuclear matrix element for  $\nu$ less double beta decay, Universe, **6**, 225 (2020).
- [45] K. Muto, E. Bender, and H.V. Klapdor, Effects of Ground State Correlations on 2 Neutrino Beta Beta Decay Rates and Limitations of the Qrpa Approach, Z. Phys. **334** 187 (1989).
- [46] D.L. Fang, B.A. Brown, and F. Simkovic, Nuclear shell model study of neutrinoless double beta decay under Left-Right symmetry model, arXiv 2407.02795v1.
- [47] H. Ejiri, L. Jokiniemi and J. Suhonen, Nuclear matrix elements for  $\beta\beta$  decays and spin isospin giant resonances, Phys. Rev. C. **105**, L022501 (2022).
- [48] H. Ejiri and S.R. Elliott, Charged current neutrino cross sections for solar neutrinos, and background to  $\beta\beta(0\nu)$  experiments, Phys. Rev. C **89** 055501 (2014).
- [49] H. Ejiri and S.R. Elliott, Solar neutrino interactions with the double- $\beta$  decay nuclei of  $^{82}\text{Se}$ ,  $^{100}\text{Mo}$ , and  $^{150}\text{Nd}$ , Phys, Rev. C **95** 055501 (2017).
- [50] J. Ferretti, R.M. Vsevolodovna, J. Kotila, and E. Santopinto,  $0^+ \rightarrow 2^+$  neutrinoless double - $\beta$  decay of  $^{76}\text{Ge}$ ,  $^{82}\text{Se}$ ,  $^{130}\text{Te}$ , and  $^{136}\text{Xe}$  in the microscopic interacting boson model, arXiv:2301.02007v1 (2023).